PERGAMON

International Journal of Heat and Mass Transfer 44 (2001) 4235–4243

International Journal of HEAT and MASS TRANSFER

www.elsevier.com/locate/ijhmt

A numerical investigation of louvered fin-and-tube heat exchangers having circular and oval tube configurations

Jin-Sheng Leu, Min-Sheng Liu, Jane-Sunn Liaw, Chi-Chuan Wang *

Energy and Resources Laboratories, Industrial Technology Research Institute, Hsinchu 310, Taiwan, ROC

Received 9 September 2000; received in revised form 8 February 2001

Abstract

A numerical investigation of the airside performance for fin-and-tube heat exchanger having circular and oval configuration is presented in this study. The geometrical parameters of louver angle, louver pitch, and louver length are examined. For a fixed louver length (6.25 mm) and louver angle (14°), a 10% decrease of heat transfer performance is observed and a 41% decrease of pressure drop is seen for oval tube configuration. The calculated results indicate that the pressure drops always with increase in louver angle. However, an optimal value of heat transfer performance is observed due to the difference in the development of thermal boundary layer on the upper and lower louver surface. Both the heat transfer and friction performance increase with louver length. However, the rate of the increase of heat transfer performance is about the same as the increase of pressure drops. © 2001 Elsevier Science Ltd. All rights reserved.

Keywords: Fin-and-tube heat exchanger; Louver fin; Oval tube

1. Introduction

Fin-and-tube heat exchangers are commonly used in the process and HVAC&R (heating, ventilating, air-conditioning, and refrigeration) industries. For HVAC&R application, the fin-and-tube heat exchangers include a group of fins arranged parallel to one another at predetermined spacing. A plurality of heat exchanger tubes were arranged in one or more rows that is perpendicular to the direction of air. The configurations of tubes can be either circular, flat, or oval. For typical applications, the airside resistance generally comprises over 90% of the total thermal resistance. Therefore, enhanced surfaces were often employed to effectively improve the overall performance of the fin-and-tube heat exchangers. The most comprehensive design database of the compact surfaces, though containing relatively old data, is the monograph by Kays and London [1]. For more advanced fin surface, the louver fin pattern is one of the most common enhanced surfaces because it can provide periodical renewal of the boundary layer. For louver fin having flat tube configurations, extensive experimental data were reported by Davenport [2], Chang and Wang [3], and Achaichia and Cowell [4]. Recently, a general heat transfer and friction correlation was proposed by Chang and Wang [5] and Chang et al. [6]. With respect to louvered fin-and-tube heat exchangers having circular tube configuration (Fig. 1), Wang et al. [7] also compiled test results from 49 samples and had developed a generalized heat transfer and friction correlation.

In addition to the experimental study, there are also some numerical investigations related to the airside performance of louver fin geometry [8–12]. These investigations provided valuable information of the fundamental phenomenon of the louver fin geometry. Several studies were concerning the geometrical effect on the flow field for fin-and-tube heat exchangers having oval and circular tube configurations [13–15]. However, the previous studies were focused on the plain fin geometry and based on the assumption of isothermal condition of the whole louver fin surfaces (i.e., the thermal conductivity of the fin is infinite). Hence, one of the main objectives of this study is to enlarge the scope

* Corresponding author. Tel.: +886-3-5916294; fax: +886-3-5820250; Bldg. 64, 195-6, Section 4, Chung Hsing Road, Chutung, Hsinchu 310, Taiwan.

E-mail address: ccwang@itri.org.tw (C.-C. Wang).

0017-9310/01/$ - see front matter © 2001 Elsevier Science Ltd. All rights reserved.
PII: S0017-9310(01)00081-3

Nomenclature

A	Z-direction length of computation domain
B	Y-direction length of computation domain
D_c	circular tube diameter, mm
H	fin pitch, mm
h	local heat transfer coefficient, W m^{-2} K^{-1}
k	thermal conductivity, W m^{-1} K^{-1}
L	louver length, mm
L_p	louver pitch, mm
N_l	louver number of fin surface
Nu	Nusselt number
n	dimensionless coordinate normal to fin surface
P	fluid pressure, Pa
ΔP	pressure drop, Pa
Pr	Prandtl number
q''	heat flux, W m^{-2}
Re_H	Reynolds number based on fin pitch
T	temperature, °C
T_{in}	air inlet temperature, °C
U_i, U_j	dimensionless velocity vector
V_{fr}	air frontal velocity, m s^{-1}
U, V, W	dimensionless velocity
X, Y, Z	dimensionless coordinates

Greek symbols

Θ	dimensionless temperature, $= (T - T_w)/(T_{in} - T_w)$
θ	louver angle, deg
ρ	fluid density, kg m^{-3}
v	kinematic viscosity, N s m^{-3}

Subscripts

b	bulk mean temperature
c	circular tube
f	fluid
o	oval tube
s	fin surface
w	tube wall

of previous investigations about the complex interactions of the louver fin within circular and oval tube bundle. The effect of finite thermal conductivity of louver fins is taken into account. This will simulate a more practical boundary conditions.

The heat transfer performance is strongly related to the geometrical design. Achaichia et al. [16] and Marchal [17] presented the flow and skin friction characteristics of louver and convex-louver fin geometry using a finite volume solver. Though they included the effect of finite fin thickness and other geometrical parameters, their analyses were based on a two-dimensional numerical scheme. In view of the previous investigations, another objective of this study is to examine the effects of louver angle, louver pitch, and louver length on the thermal-hydraulic characteristics of fin-and-tube heat exchangers with oval tubes based on a three-dimensional numerical scheme.

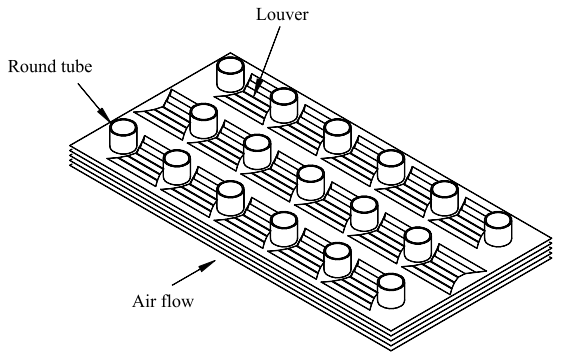

Fig. 1. Louvered fin-and-tube heat exchangers having circular tube configuration.

2. Mathematical analysis

Fig. 2 shows the computational domain and coordinate system used in the present study. Calculations were performed in a unit cell as depicted in Fig. 2(b). The flow along the top and bottom surfaces of the mesh is assumed periodic. The fluid is considered incompressible with constant properties and the flow over the louvers is assumed to be laminar in the steady-state. The dimensionless equations for continuity, momentum and energy both in flow region and in fin region may be expressed in tensor form as

(1) Flow region:

$$\frac{\partial U_i}{\partial X_i} = 0, \tag{1}$$

$$\frac{\partial}{\partial X_i}(U_i U_j) = -\frac{\partial P}{\partial X_i} + \frac{1}{Re_H}(\nabla^2 U_i), \tag{2}$$

$$\frac{\partial}{\partial X_i}(\Theta_f U_j) = \frac{1}{Re_H Pr}(\nabla^2 \Theta_f). \tag{3}$$

(2) Fin region:

$$\frac{\partial^2 \Theta_s}{\partial X_j^2} = 0. \tag{4}$$

The dimensionless temperature is defined as $\Theta = (T - T_w)/(T_{in} - T_w)$. The subscripts f and s denote the

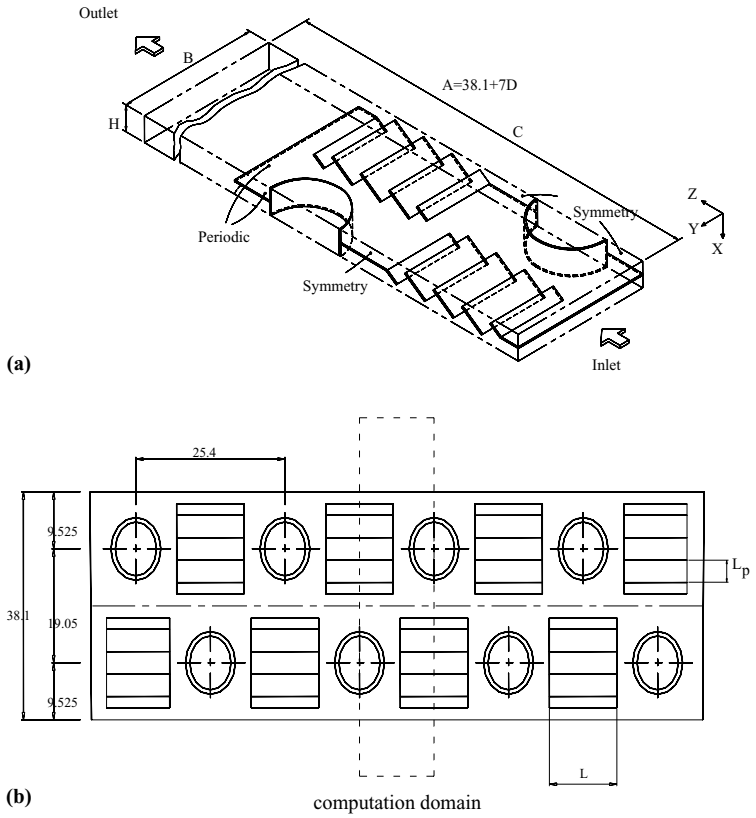

Fig. 2. Schematic of the computational domain.

temperature of fluid and fin surface, respectively. The frontal velocity V_{fr}, fin spacing H, and velocity pressure ρV_{fr}^2 were employed in the non-dimension characteristics of velocity, length, and pressure. The Reynolds number is defined as $Re_H = V_{fr}H/v$.

As depicted in Eqs. (2)–(4), the governing equations are elliptic in the spatial coordinates, hence boundary conditions are required for all boundaries of the computation domain. In addition, one more pair of boundary conditions for the velocity and thermal fields needs to be specified on the interface of fin surface and fluid due to the consideration of the conjugate heat transfer between the louver fin and fluid. These boundary conditions are described as follows:

(1) The upstream boundary:

$$U = V = 0, \quad W = 1, \quad \Theta_f = 1.$$

(2) The downstream boundary: (located seven tube diameters after the exit of the heat exchanger)

$$P = 0, \quad \partial U/\partial Z = \partial V/\partial Z = \partial W/\partial Z = \partial(\Theta_f/\Theta_b)/\partial Z = 0.$$

(3) The wing boundaries (Y–Z, X–Z planes):

For Y–Z planes, periodic boundary:

$$U(0,Y,Z) = U(H,Y,Z), \quad V(0,Y,Z) = V(H,Y,Z), \quad W(0,Y,Z) = W(H,Y,Z),$$

$$\Theta_f(0,Y,Z) = \Theta_f(H,Y,Z).$$

For X–Z planes, symmetric boundary:

$$V = 0, \quad \partial P/\partial Y = \partial U/\partial Y = \partial W/\partial Y = \partial \Theta_f/\partial Y = 0.$$

(4) The tube wall surfaces: (no-slip conditions)

$$U = V = W = 0, \quad \Theta_f = 0.$$

(5) The fin surfaces:

$$\Theta_f = \Theta_s, \quad k_f \partial \Theta_f/\partial n = k_s \partial \Theta_s/\partial n, \quad U = V = W = 0.$$

(6) The contact region between fin and tubes:

$$U = V = W = 0, \quad \Theta_s = \Theta_w = 0.$$

The local heat transfer coefficient h is defined as

$$h = \frac{q''}{T_s - T_b}, \tag{5}$$

where q'' is the local heat flux and T_b is the local bulk mean temperature. The local heat transfer coefficient can be expressed in terms of Nusselt number, Nu, i.e.,

$$Nu = \frac{hH}{k} = \frac{\partial((T - T_s)/(T_b - T_s))}{\partial n}. \quad (6)$$

The average Nusselt number is calculated from the local Nusselt number with Eq. (6), i.e.,

$$\overline{Nu} = \frac{\int\int Nu\,dx\,dy}{\int\int dx\,dy}. \quad (7)$$

Then we can get the average heat transfer coefficient $\bar{h} = \overline{Nu}k/H$.

3. Numerical methods

The preceding set of equations was solved by a commercially available computer software (PHOENICS 3.1 1998) [18]. A sufficiently fine grid-size, $30 \times 60 \times 400$ grid points, is adopted as the computational domain. A thorough check of the grid independence for the numerical solutions was performed to ensure the accuracy and validity of the numerical results. Several algorithms (SIMPLE, SIMPLER, SIMPLEST) for calculating the pressure field are available in the computer software. The SIMPLEST algorithm was finally adopted since SIMPLEST algorithm shows much better convergent characteristics during the refinement of grids. The governing equations are discretized with hybrid scheme. The criterion of convergence in this study is when the global residual is less than 0.01. Computations were performed on a HP/750 workstation. Typical CPU time is about 8 h for each case.

4. Results and discussion

Fig. 3 shows the comparisons of the average Nusselt number and pressure drop between the numerical and experimental results. To ensure the numerical results are reliable, calculations were first made to examine the performance of a louver fin geometry having circular tube configuration with the experimental data by Wang et al. [19]. The detailed geometry of the examined heat exchanger is given as follows.

Tube outside diameter (include fin thickness)	10.42 mm
The number of tube row	2
Longitudinal tube pitch (P_l)	19.05 mm
Transverse tube pitch (P_t)	25.4 mm
Fin thickness	0.115 mm
Fin pitch	2.06 mm
Louver angle (θ)	14°
Louver pitch (L_p)	3.75 mm
Louver length (L)	6.25 mm
Approximate tube temperature	60°C

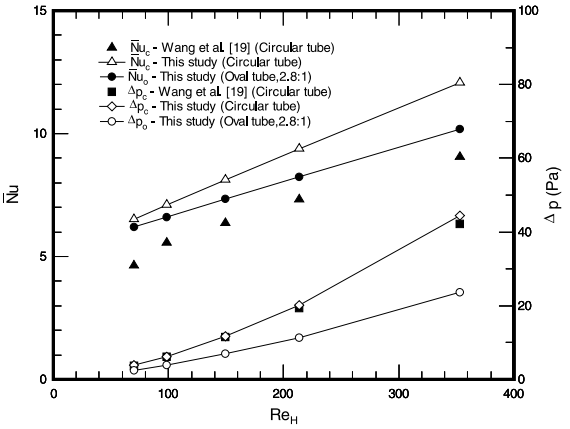

Fig. 3. Comparison of the louver fin results with the experimental data by Wang et al. [19].

Inlet air temperature	30°C
Inlet frontal velocity	0.5–2.6 m s^{-1}
Air density	1.189 kg m^{-3}
Fin material	Aluminum, $k = 204$ W m^{-1} K^{-1}

As seen in the figure, the numerical predictions of the pressure drops are in excellent agreement with the experimental results. The tendency of the Nusselt number vs Reynolds number Re_H for the numerical results is similar to those of experimental results but is different in magnitude. Actually, the numerical results overestimated the average Nusselt number by approximately 20–30%. The results are analogous to those reported by Achaichia et al. [20] and Atkinson et al. [10]. Atkinson et al. [10] performed a three-dimensional numerical analysis for louvered fin array in compact heat exchanger using STAR-CD commercial code. Their heat transfer coefficients are about 15–25% higher than the associated experimental results. There are some possible explanations about the overestimation. Firstly, the actual boundary condition on the tube surface is not constant during the experiment. Secondly, the contact resistance between the tube and fin collar, which is not accounted for in the numerical simulation, is absorbed to the measured heat transfer coefficients during the experiments.

In addition to the circular tube configuration, the oval tube (or flat tube) was often employed as an alternative to the design of fin-and-tube heat exchangers. From the consideration of thermal hydraulics, the oval tube geometry offers significant advantages over the circular tube in the following aspects as depicted by Webb and Jung [21]:

1. The air flow is normal to all of the narrow strips and the wake dissipation length is smaller.
2. A low wake region occurs behind the tubes.
3. It provides higher fin efficiency.

4. The low projected area of the oval tube will result in lower profile drag.

Thus, it is interesting to examine the airside performance for the oval tube configuration. In this study, we had examined the effect of axis ratio on the airside performance for the oval fin-and-tube heat exchangers with and without louvers. For comparison purpose, the perimeter of the oval tube is equal to that of the circular tube ($D = 10.42$ mm). The specific geometric dimensions for calculation are $F_p = 2.06$ mm, $P_l = 19.05$ mm, $P_t = 25.4$ mm, $\theta = 14°$, $L = 6.25$ mm, $L_p = 3.75$ mm ($N_l = 4$), and $Re_H = 149.4$. Results for the louver fin are in terms of ratios of $\bar{h}_o/\bar{h}_c$, $\Delta p_o/\Delta p_c$, and $(\bar{h}_o/\Delta p_o)/(\bar{h}_c/\Delta p_c)$. As seen in Fig. 4, for louver fin configuration, the heat transfer coefficients for oval tube are lower than those of the circular tube configuration and decrease with increase of axis ratio. The pressure drops for oval tube configuration, as expected, decrease with axis ratios. For an axis ratio of 2.8:1, the heat transfer coefficient for oval tube is less than its circular tube counterpart by approximately 10%. However, the pressure drop for the circular tube configuration exceeds the results of the oval tube by 41%. The efficiency index, which is evaluated as $(\bar{h}_o/\Delta p_o)/(\bar{h}_c/\Delta p_c)$, is always increased with increase of axis ratio. The results indicated that the oval tube with louver fin might be more beneficial due to its superior performance especially in frictional characteristics.

For the results of plain fin geometry, similar results for pressure drops are observed in Fig. 5 (axis ratio = 2.8). The pressure drops are significantly lower for the oval tube. Notice that, for $Re_H = 353.2$, the pressure drops for circular tube exceed oval tube by more than 100%! This is because the percentage of the form drag caused by the tube is comparatively large when compared to the louver fin geometry. Results of heat transfer performance are, however, different from those of louver

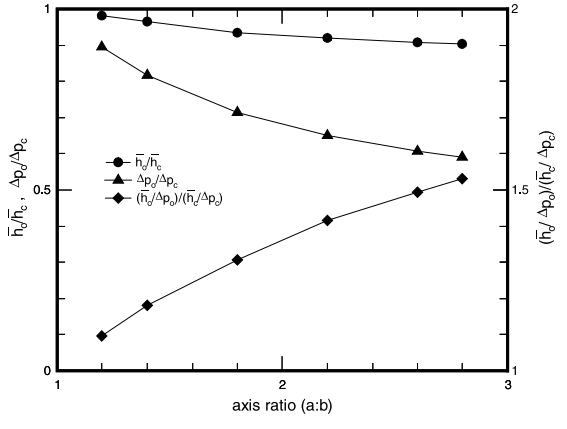

Fig. 4. Ratios of $\bar{h}_o/\bar{h}_c$, $\Delta p_o/\Delta p_c$, and $(\bar{h}_o/\Delta p_o)/(\bar{h}_c/\Delta p_c)$ at $Re_H = 149.4$.

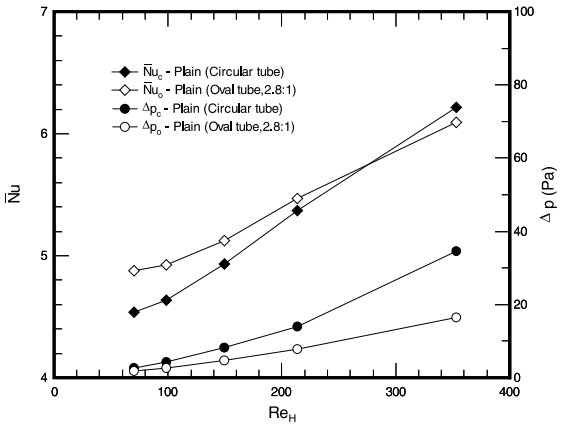

Fig. 5. Airside performance for circular/oval fin-and-tube heat exchangers having plain fin configuration.

fin geometry. The plain fin geometry with oval tube reveals higher heat transfer coefficients when Re_H is less than about 275 and decrease when Re_H is larger than 275. Comparing the results of louver fin shown in Fig. 4, one can see that the heat transfer characteristics for plain fin are quite different. To further quantify this phenomenon, detailed variations of the heat transfer performance within the heat exchangers should be examined.

Fig. 6 shows the variations of span-averaged Nusselt number on the X–Y plane along the streamwise direction (Z direction). Results for plain fin at $Re_H = 70.3$ and 353.2 are drawn in the figure. For comparison purpose, the results of louver fin at $Re_H = 149.4$ are also depicted in the figure. For the plain fin geometry at $Re_H = 70.3$, both circular and oval tube experience a detectable decrease of heat transfer performance at the rear of the first tube due to the wake formation. The mean heat transfer performance for the oval tube configuration at the first row is superior to the circular tube configuration. However, one can see that there is no appreciable difference in the second row. This is due to the boundary layer being thermally fully developed. For $Re_H = 353.2$, similar results are observed at the first row. Though the mean heat transfer characteristics for oval tube at the first row is still slightly higher than those of circular tube, however, one can see that the circular tube configuration offers much higher heat transfer performance at the contraction region of the second row. Thus, a slightly higher mean heat transfer performance is observed for the circular tube configuration at a higher Reynolds number (353.2). Fig. 6(c) also depicts the Nusselt number distribution for the louver fin geometry at $Re_H = 149.4$. Unlike those of plain fin geometry, the average Nusselt number for circular tube configuration is slightly higher than those of oval tube. This is valid for first and second rows.

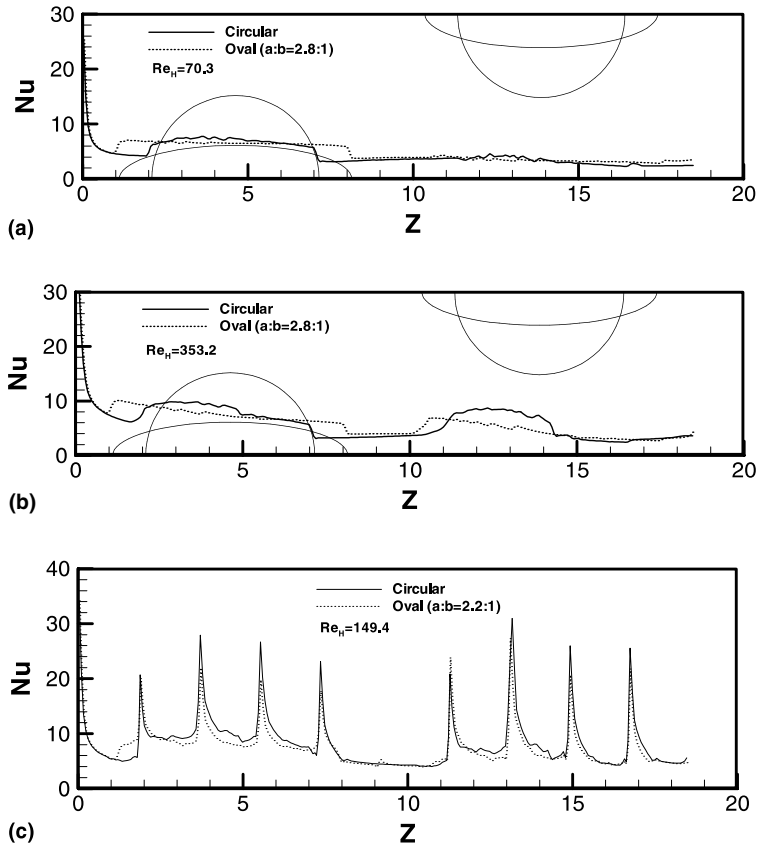

Fig. 6. Variations of span-averaged Nusselt number on the X–Y plane along the streamwise direction: (a) plain fin with $Re_H = 70.3$; (b) plain fin with $Re_H = 353.2$; (c) louver fin with $Re_H = 149.4$.

Apparently, the presence of louver may effectively directs the air flow and results in sharp rise of local Nusselt number. In this case, there are four louvers in each row along the streamwise direction. Thus, one can see four local maximums of the Nusselt number that occurs at the leading edge of the louver. It should be pointed out that the associated highest value occurs at the second louver in each row. This is due to the additional contribution caused by the tube.

Fig. 7 shows the effect of louver angle (θ) on the airside performance of louver fin geometry. Calculations were made at $Re_H = 149.4$ for three louver pitches ($L_p = 3.75,\ 2.68$, and 2.08 mm) with an axis ratio of 2.2 and $L = 8.37$ mm. As seen in the figure, the pressure drops increase with louver angle for all three louver pitches. The increasing trend is especially significant as the louver pitch is reduced to 2.68 or 2.08 mm. Fig. 7 also shows that smaller louver pitch would result in better heat transfer performance. This is attributable to periodic renewal of the boundary layer. However, it is noted that the benefit of smaller louver pitch may be offset by higher pressure drop. In addition, Fig. 7 indicates the relation between the average Nusselt number

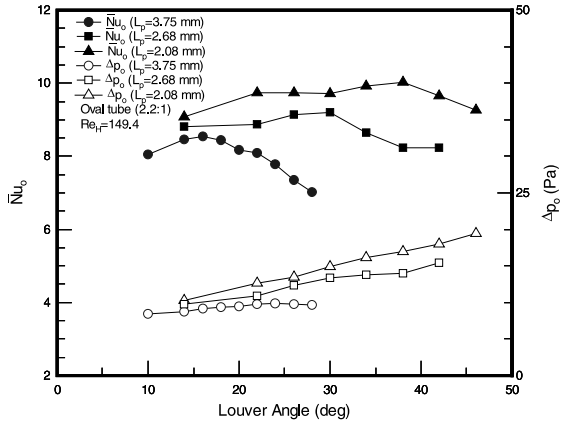

Fig. 7. Heat transfer performance and pressure drop vs louver angle for three specific louver pitch with axis ratio = 2.2 and $Re_H = 149.4$.

and the louver angle is much more complex. One can observe a "maximum" phenomenon of average Nusselt number to change of louver angle. This phenomenon is especially pronounced for $L_p = 3.75$ mm. The calculated

Table 1
Relation between θ_{max} and L_p at $Re_H = 149.4$

L_p (mm)	Range of θ for calculation (°)	θ_{max} (°)
3.75	10–28	16
2.68	14–42	30
2.08	14–46	38

results of the maximum louver angle for various louver pitches are tabulated in Table 1.

Detailed examinations of the maximum phenomenon are elaborated as follows. Kajino and Hiramatsu [22] observed that the boundary layers exist on both the upper and lower surfaces of the louver surface. They concluded that relevant heat transfer enhancement is due to the thin boundary layers that form at the leading edge of each louver. Apparently the development of the boundary layer on the upper and lower surfaces should be different due to the presence of louver angle. In general, the upper surface that receives the impinging airflow directly may result in an effect of "thinning" the thermal boundary layer, and the lower surface is acting as "diffusing" that may thicken the thermal boundary layer. To further quantify the present arguments, details of the isotherm pattern for $L_p = 3.75$ mm at $\theta = 10°$, 16°, and 26° of the first row are shown in Fig. 8. As illustrated in Fig. 8(c), for $\theta = 26°$, the regions of upper surfaces possess stronger temperature gradient than the other two cases. However, the temperature gradient at the regions of lower surfaces for $\theta = 26°$ is smaller than those of $\theta = 10°$ and 16°. The results implies a slight variation (may be slight increase or slight decrease) of the heat transfer performance at the upper louver surface while a significant drop of the heat transfer performance at the

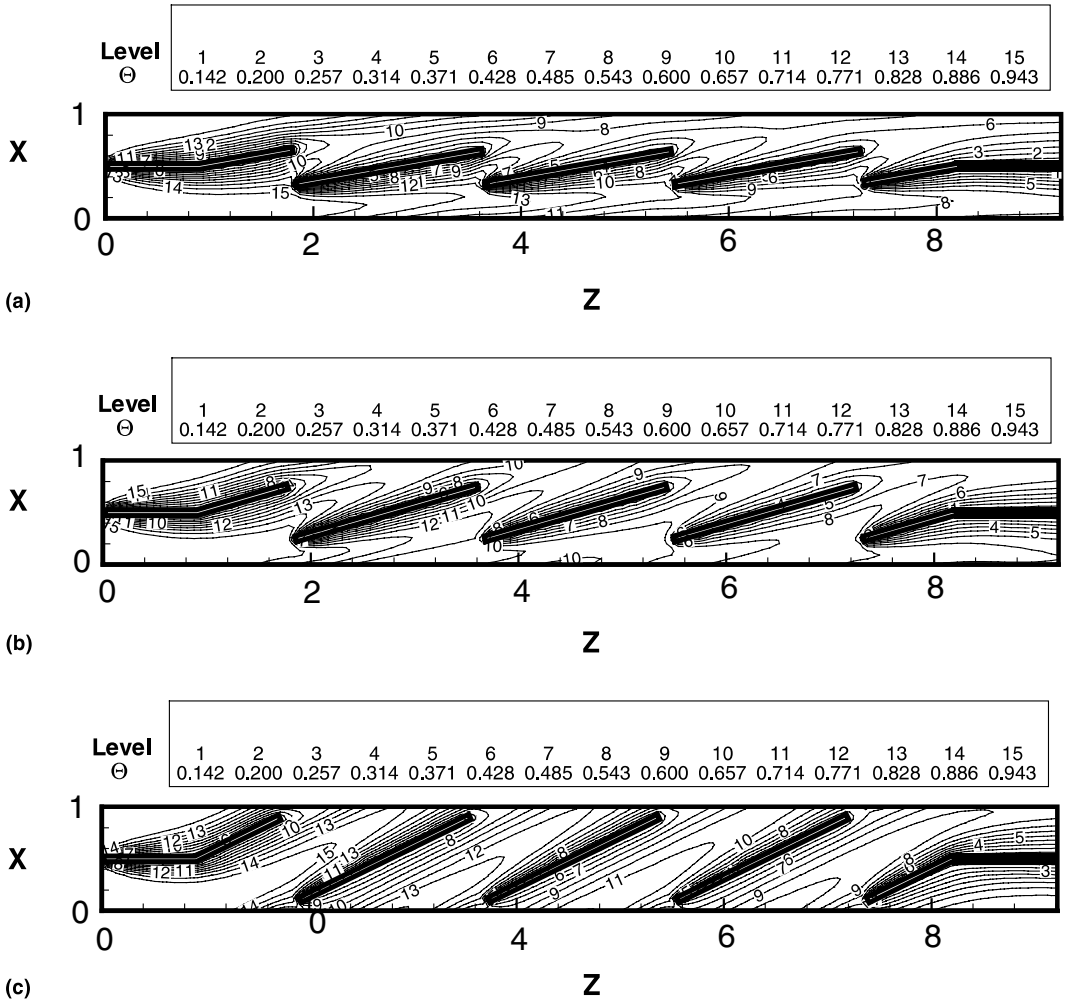

Fig. 8. Isotherm patterns on the louver regions for $\theta = 10°$, 16°, and 26° with axis ratio = 2.2, $L_p = 3.75$ mm, and $Re_H = 149.4$.

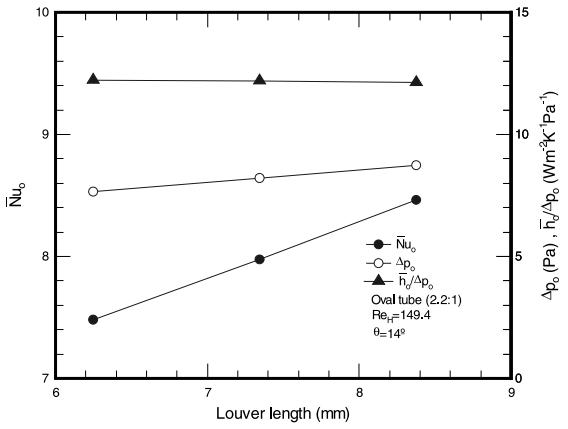

Fig. 9. Heat transfer performance and pressure drop vs louver length with axis ratio = 2.2, $\theta = 14°$, and $Re_H = 149.4$.

lower surface when the louver angle is increased. In this connection, summation of the heat transfer performance of the upper and lower fin may result in a maximum phenomenon. The maximum phenomenon due to the effect of louver angle suggests a pronounced drop of $\bar{h}_o/\Delta P_o$ vs louver angle.

Fig. 9 shows the numerical results of average Nusselt number and pressure drop for three different louver lengths L (6.25, 7.34 and 8.37 mm) at axis ratio = 2.2, $Re_H = 149.4$, and $\theta = 14°$. As seen in figure, both Nusselt number and pressure drop increase with increase of louver length. Surprisingly, the rate of increase of heat transfer performance is approximately equal to that of pressure drop. For example, the heat transfer performance for $L = 8.37$ mm is about 13.1% higher with a penalty increase of pressure drop of 13.2%. Eventually, one can observe a nearly constant value of $\bar{h}_o/\Delta P_o$ vs louver length. The results are different from those of the effect of louver angle that shows a pronounced drop of $\bar{h}_o/\Delta P_o$ vs louver angle. Part of the explanation is because the airflow is more effectively directed by the increase of louver length. In addition, the pressure field is comparatively insensitive to change of spanwise direction when compared to the streamwise direction. Hence, the increase of pressure drop is moderate since the fin pitch is fixed in this calculation. The conclusion drawn in this calculation reveals the beneficial part of increase of louver length. However, for practical application, the maximum louver length cannot exceed the distance between neighboring tubes.

5. Conclusions

In this study, a three-dimensionally numerical investigation into the thermal hydraulic characteristics of louvered fin-and-tube heat exchangers with circular and oval tube is presented. The effects of axis ratio, louver pitch, louver angle, and louver length were examined in this study. Major conclusions are summarized as follows:

1. For a fixed louver length and louver angle, results of various axis ratio (1.2–2.8) indicated that both the heat transfer performance and pressure drops decrease with increase of axis ratio. For $Re_H = 149.4$ and axis ratio of 2.8, a 10% decrease in heat transfer performance is observed and a 41% decrease of pressure drop is seen for oval tube configuration.
2. For the plain fin configuration and $Re_H < 275$, the heat transfer performance for oval tube is slightly higher than those of circular tube geometry. However, the heat transfer performance is reversed when $Re_H > 275$. It should be further pointed out that the heat transfer performance for oval tube at the first row is always superior to the circular tube configuration regardless change of the Reynolds number. The pressure drops for the oval tube are much smaller for plain fin geometry owing to the comparatively small form drag of oval tube.
3. For a fixed geometrical parameters, both the heat transfer performance and pressure drops increase with decrease of louver pitch.
4. The pressure drops increase consistently with louver angle. However, for the relation of heat transfer performance to louver angle, an optimum value is observed. This optimum value is associated with the difference of development of boundary layer on the upper and lower surface of louver.
5. Both heat transfer performance and friction increase with louver length. Surprisingly, the rate of increase of heat transfer performance is about the same as the increase of pressure drop. Accordingly, no detectable change of $\bar{h}_o/\Delta P_o$ vs louver length is observed.

Acknowledgements

The authors would like to express gratitude for the Energy R&D foundation funding from the Energy Commission of the Ministry of Economic Affairs, Taiwan for providing the financial supports of the current study.

References

[1] W.M. Kays, A.L. London, Compact Heat Exchangers, third ed., McGraw-Hill, New York, 1984.
[2] C.J. Davenport, Correlation for heat transfer and flow friction characteristics of louvered fin, AICHE Symp. Ser. 79 (1983) 19–27.
[3] Y.J. Chang, C.C. Wang, Air side performance of brazed aluminum heat exchangers, J. Enhanced Heat Transfer 3 (1996) 15–28.

[4] A. Achaichia, T.A. Cowell, Heat transfer and pressure drop characteristics of flat tube and louvered plate fin surfaces, Exp. Thermal Fluid Sci. 1 (1988) 147–157.
[5] Y.J. Chang, C.C. Wang, A generalized heat transfer correlation for louver fin geometry, Int. J. Heat Mass Transfer 42 (1997) 1945–1956.
[6] Y.J. Chang, K.C. Hsu, Y.T. Lin, C.C. Wang, A generalized friction correlation for louver fin geometry, Int. J. Heat Mass Transfer 43 (2000) 2237–2243.
[7] C.C. Wang, C.J. Lee, C.T. Chang, S.P. Lin, Heat transfer and friction correlation for compact louvered fin-and-tube heat exchangers, Int. J. Heat Mass Transfer 42 (1999) 1945–1956.
[8] D.K. Tafti, G. Wang, W. Lin, Flow transition in a multi-louvered fin array, Int. J. Heat Mass Transfer 43 (2000) 909–919.
[9] H. Matsushima, T. Hatada, T. Endo, T. Senshu, Three dimensional simulation of forced convection and heat transfer in heat exchangers with convex strip fins by the finite element method, in: ASME National Heat Transfer Conference, Minneapolis, MN, 1991, pp. 1–5.
[10] K.N. Atkinson, R. Drakulic, M.R. Heikal, T.A. Cowell, Two- and three-dimensional numerical models of flow and heat transfer over louvered fin arrays in compact heat exchangers, Int. J. Heat Mass Transfer 41 (1998) 4063–4080.
[11] S.F. Tsai, T.W.H. Sheu, S.M. Lee, Heat transfer in conjugate heat exchanger with a wavy fin surface, Int. J. Heat Mass Transfer 42 (1999) 1735–1745.
[12] C.H. Bemisderfer, Heat transfer: a contemporary analysis tool for developing improved heat transfer surfaces, ASHRAE Trans. 93 (1) (1987) 1157–1167.
[13] J.Y. Jang, J.Y. Yang, Experimental and 3-D numerical analysis of the thermal-hydraulic characteristics of elliptic finned-tube heat exchangers, Heat Transfer Eng. 19 (4) (1998) 55–67.
[14] H.M. Badr, Mixed convection from a straight isothermal tube of elliptic cross section, Int. J. Heat Mass Transfer 37 (1994) 2343–2365.
[15] T. Ota, H. Nishiyama, Y. Taoka, Heat transfer and flow around an elliptic cylinder, Int. J. Heat Mass Transfer 27 (1984) 1771–1779.
[16] A. Achaichia, M.R. Heikal, Y. Sulaiman, Numerical investigation of flow and friction in louvered fin arrays, in: The 10th Heat Transfer Conference, vol. 4, 1994, pp. 333–338.
[17] D. Marchai, A. Bensafi, Optimal design of enhanced fins for fin-and-tube heat exchangers: application to a convex-louver fin, in: Proceedings of the International Conference and Exhibit on Heat Exchangers for Sustainable Development, Lisbon, Portugal, 1998, pp. 129–137.
[18] PHOENICS user's Guide, Version 3.1, CHAM, Bakery House, 40 High Street, Wimbledon Village, London, UK, 1998.
[19] C.C. Wang, Y.P. Chang, K.U. Chi, Y.J. Chang, A study of non-redirection louver fin-and-tube heat exchangers, in: Proceeding of Institute of Mechanical Engineering Part C, vol. 212, 1998, pp.1–14.
[20] A. Achaichia, T.A. Cowell, Heat transfer and flow friction characteristics of flat tube and louvered plate fin surfaces, Exp. Thermal Fluid Sci. 1 (1988) 147–157.
[21] R.L. Webb, S.H. Jung, Air-side performance of enhanced brazed aluminum heat exchangers, ASHRAE Trans. 98 (2) (1992) 391–401.
[22] M. Kajino, M. Hiramatsu, Research and development of automotive heat exchangers, Heat Transfer in High Technology and Power Engineering Hemisphere, Washington, DC, 1987, pp. 420–432.